Published in Eclogae Geologicae Helvetiae 96 : 2003
which should be used for any reference to this work

Brittle orogen-parallel extension in the internal zones of the Swiss Alps (South Valais)

CHAMPAGNAC JEAN-DANIEL[1], SUE CHRISTIAN, DELACOU BASTIEN, AND BURKHARD MARTIN.

Keywords: Swiss Alps, brittle extension, paleostress analysis, morphotectonics, recent faulting

ABSTRACT

The latest Alpine faulting is examined in the Valais region of the Swiss Alps. We used satellite imagery and a 25m Digital Elevation Model to identify and map geomorphic features such as fault scarps and lineaments. Verification, fault characterization and fault planes / striae measurements for paleostress analysis were conducted in the field. We identified three fault families that post-date nappe emplacement, E-W, NE-SW and NW-SE oriented. A large majority of faults are normal, with some strike slip component. The normal / dextral Rhône fault system controls the brittle deformation close to the Rhône valley, where it is morphologically well expressed. This regional brittle deformation was analysed using paleostress inversion methods at 56 measurement sites. The extensional axis σ3 is regionally consistent with a NE-SW (N65°) orientation. The deformation regime, based on the ellipsoid form parameter $\Phi = (\sigma2-\sigma3)/(\sigma1-\sigma3)$, varies between radial extension ($\Phi=0$) and transtension ($\Phi=1$). This orogen-parallel extension, similar to the major "Simplon fault" kinematics, is documented over a large area of the northwestern Alps: in the hangingwall of the Simplon fault, in the Southern Valais area, and in the Aosta valley region.

RESUME

De nouvelles données de fracturation tardi-alpine dans le Sud Valais (Alpes Suisse) sont présentées ici. Nous avons utilisé différentes images satellites ainsi que le Modèle Numérique de Terrain (MNT) à 25m de résolution pour identifier et cartographier différentes structures morphologiques, linéaments ou escarpements de failles. Un contrôle sur le terrain nous a permis de reconnaître que ces structures sont pour la plupart des failles. Nous avons identifié trois familles de failles, orientées E-W, NE-SW et NW-SE, qui sont postérieures à la mise en place des nappes et à toutes les structures ductiles. Ces failles sont principalement normales, avec localement une composante décrochante. La faille du Rhône, normale / dextre, contrôle la déformation cassante à proximité de la vallée du Rhône, où elle présente une forte signature morphologique. Les mesures de couples failles / stries sur 56 sites nous a permis de calculer les paléocontraintes par la méthode d'inversion directe: l'axe d'extension σ3 est globalement orienté NE-SW (N65°). Le paramètre de forme de l'ellipsoïde des paléocontraintes $\Phi = (\sigma2-\sigma3)/(\sigma1-\sigma3)$, varie entre de l'extension radiale ($\Phi=0$) et de la transtension ($\Phi=1$). Cette direction d'extension, parallèle à la direction des structures alpines est compatible avec l'extension accommodée par la faille du Simplon. Elle se retrouve dans une grande partie des Alpes nord-occidentales, du Simplon au Val d'Aoste, en passant par le Sud Valais.

1. Introduction

Most of the previous studies of the alpine collisional belt have focused mainly on the contractional structures, in particular folds and thrust. This has led to several well constrained models of the Tertiary kinematics of the belt (e.g. Steck 1984, Choukroune et al. 1986, Le Pichon et al. 1988, Ménard 1988, Steck & Hunziker 1994, Mosar 1999, Steck et al. 2001) The present-day dynamics of the Alps is still a matter of debate. On the continental scale, Europe/Africa convergence is ongoing at rates from 3 to 8 mm/year in a N to NW direction at the longitude of the Alps (Argus et al. 1989, Demets et al. 1990, 1994, Albarello et al. 1995, Crétaux et al. 1998, Calais et al. 2000, Kreemer & Holt 2001, Nocquet 2002). Little, if any of this convergence is taking place in the Alps, however, some authors have proposed the western Alps to be in a post-collisional stage (Sue et al. 1999, Delacou et al. submitted).

Large scale extensional structures are documented in many parts of the Alps (e.g. Mancktelow 1985, Mancel & Merle 1987, Selverstone 1988, Ratschbacher et al. 1989, Wust & Silverberg 1989, Steck & Hunziker 1994, Frisch et al. 2000). Extensional tectonics, mostly in an orogen-parallel direction, is shown to begin early, in late Oligocene and early Miocene, at times when orogen perpendicular thrusting in external parts of the Alps is still active (Bistacchi & Massironi 2000, Tricart et al. 2001, Sue & Tricart 2002). During the last ten years, increasing attention has been paid to the latest extensional structures which took place under increasingly brittle conditions,

[1] Jean-Daniel Champagnac, Université de Neuchâtel, Institut de géologie, Rue Argand, 11, CH-2007 Neuchatel, Switzerland, Tel: (+41) 32 718 26 57, Fax: (+41) 32 718 26 01. Email: jean-daniel.champagnac@unine.ch

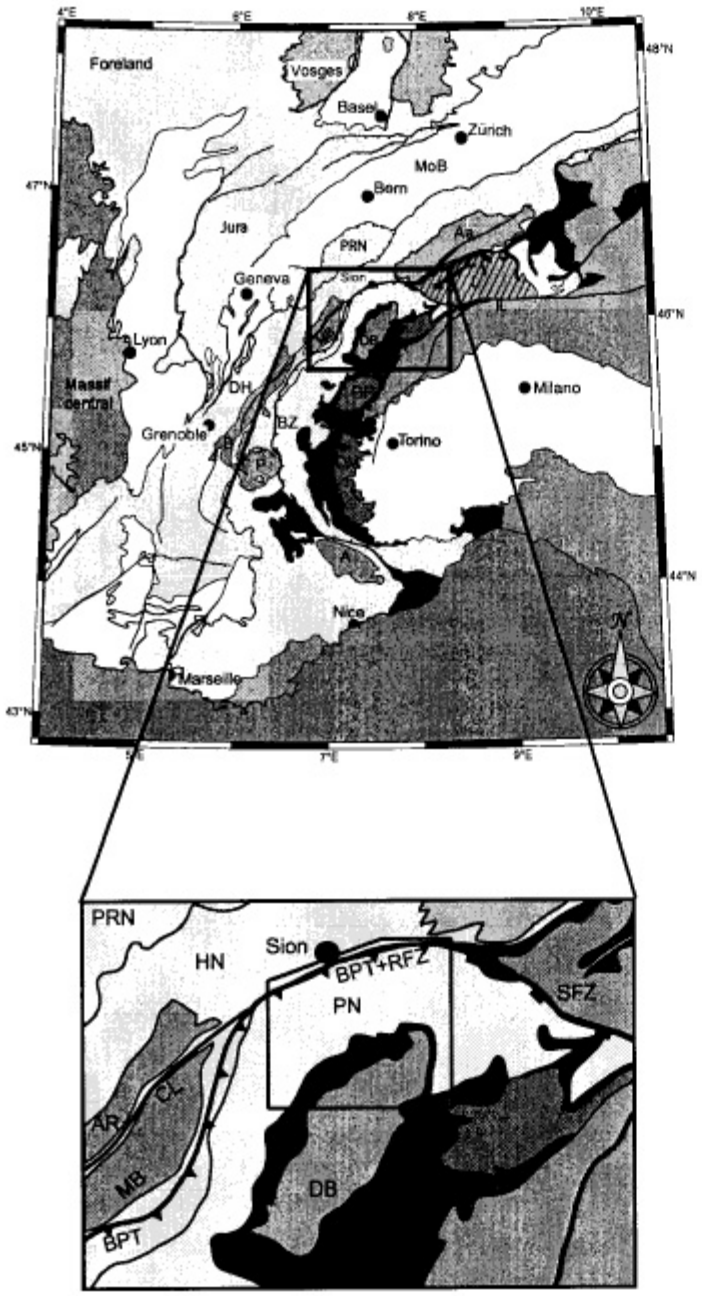

Fig. 1. Location of the studied area in the Alpine belt (black square).
Tectonic units: A: Argentera; **Aa**: Aar; **AR**: Aiguilles Rouges; **B**: Belledonne; **BZ**: Briançonnais zone; **DB**: Dent Blanche nappe; **DH:** Dauphiné / Helvetic zone; **DM:** Dora Maira; **GP**: Gran Paradiso; **HN**: Helvetic Nappes; **L**: Lepontine Dome; **MoB**: Molass Bassin; **MB**: Mont Blanc; **PZ**: Piémontais zone; **P**: Pelvoux; **PN**: Penninic nappes; **PRN**: Prealpine Nappes.
Faults zone or "lines": BPT: Basal Penninic Trust;**CL**: Chamonix Line; **IL:** Insubric line; **RFZ**: Rhône Fault Zone; **SFZ**: Simplon Fault Zone.

some of which being probably still active today (Massironi et al. 1997, Sue 1998, Sue & Tricart 1999, Bistacchi et al. 2000, Bistacchi & Massironi 2000, Sue & Tricart 2002, Grosjean et al. in press, Sue & Tricart in press).

In this paper, we analyze the brittle deformation in the South Valais area, which belongs to the internal zones of the Swiss Alps, between the Rhône valley to the north and the water divide to the south. This area lies to the South-West of the Simplon fault and can be regarded as its hangingwall (Mancktelow 1985, 1992). Our analysis is based on systematic mapping of the fault patterns, and the determination of paleostress field(s) based on a large database of fault/striae measurements.

2. Geological and tectonic setting

The studied area is located in the South Valais (Swiss Alps). It is limited to the north by the Rhône valley, to the south by the crest-line of the Valais Alps with many exceeding 4000m summits (e.g. Grand Combin, Dent Blanche, Matterhorn and Monte Rosa), to the west by the Val de Bagnes, and to the east by the Mattertal (or "Zermatt valley") (Fig. 1).

This area belongs to the internal zone of the Alps and is made up of middle Penninic nappes, also referred to as the Briançonnais zone, overridden by the main Alpine Piémontais suture zone and the Dent Blanche nappe. The Briançonnais nappes consist of slices of pre-Carboniferous basement rocks, with their cover of Permo-Carboniferous and Mesozoic sediments. The Piemontais suture zone is a melange of ophiolitic rocks and associated oceanic "schistes lustrés" calcschists. The overriding Dent Blanche nappe s.l. is the highest nappe in this part of the Western Alps. It is mainly a crystalline basement unit with small remnants of sedimentary cover (Steck 1984, Steck & Hunziker 1994, Escher et al. 1997, Steck et al. 1997). The metamorphic history of the Penninic units is complex. Parts of the Piémontais suture zone have experienced high to ultrahigh pressure metamorphism, while most of the basement units have undergone only moderate pressure, middle to upper greenschist facies only (Desmons et al. 1999, Frey et al. 1999). Peak temperatures were probably reached in the latest Eocene around 38Ma (e.g. Hunziker et al. 1992). The post peak temperature cooling history is well constrained through zircon and apatite fission track ages (Soom 1990, Hunziker et al. 1992, Seward & Mancktelow 1994).

The study area is bordered by a series of major faults or fault zones.

To the east, the Simplon fault zone has been described as a major NW-SE striking low-angle detachment with a long history, including both ductile high temperature deformation and low temperature brittle deformation features (*e.g.* Mancktelow 1985, 1990, 1992, Steck & Hunziker 1994, Grosjean et al. in press). The maximum cumulated dip-slip displacement has been estimated at around 36 km, in a top-to-the-SW direction (Mancktelow 1992, Grasemann & Mancktelow 1993, Steck & Hunziker 1994). At the scale of the Alpine orogen, the Simplon fault zone seems to be a relay between the dextral Insubric Line and the normal/dextral Rhône fault zone.

To the north, the Rhône fault zone follows closely the present-day Basal Penninic Thrust of the Valais (Steck & Hunziker 1994). The Rhône valley can be regarded as the geomorphic

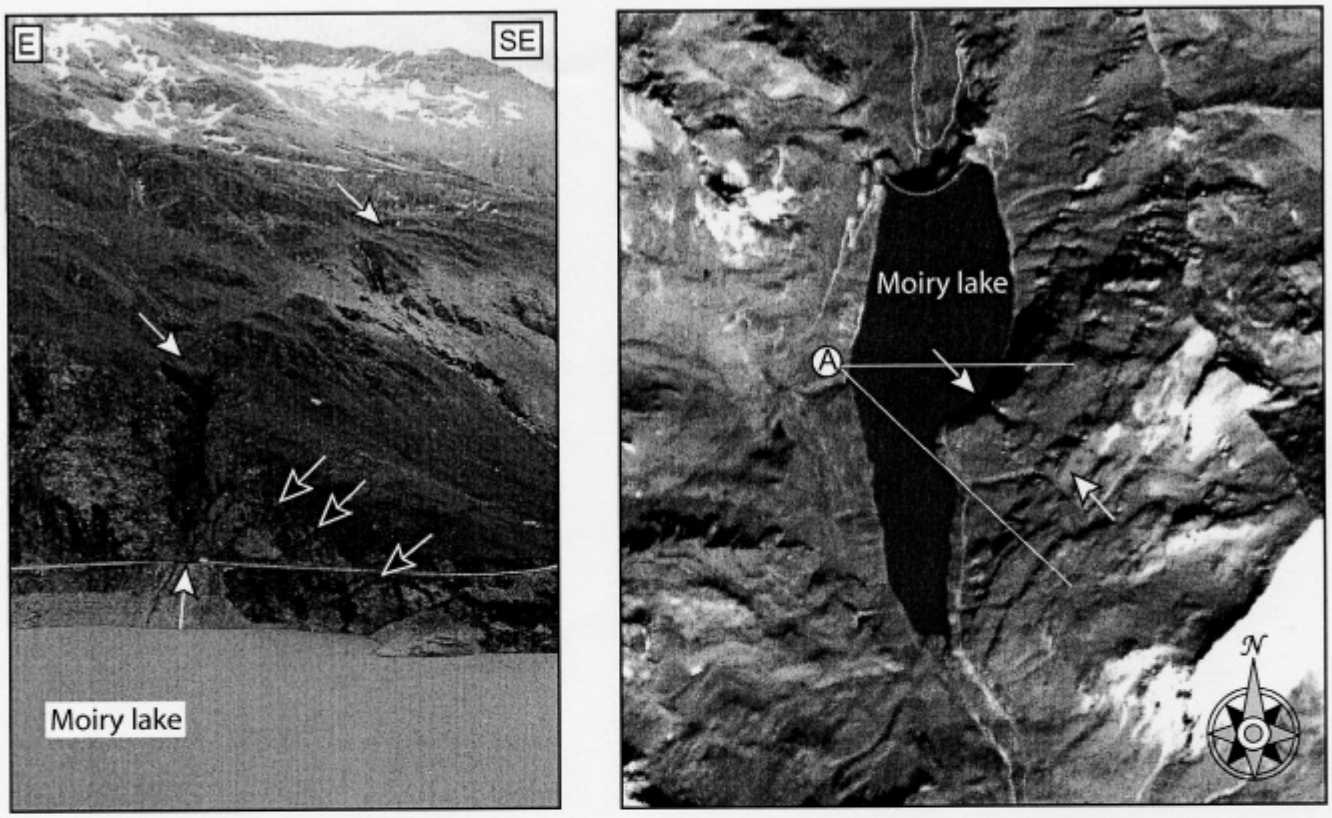

a

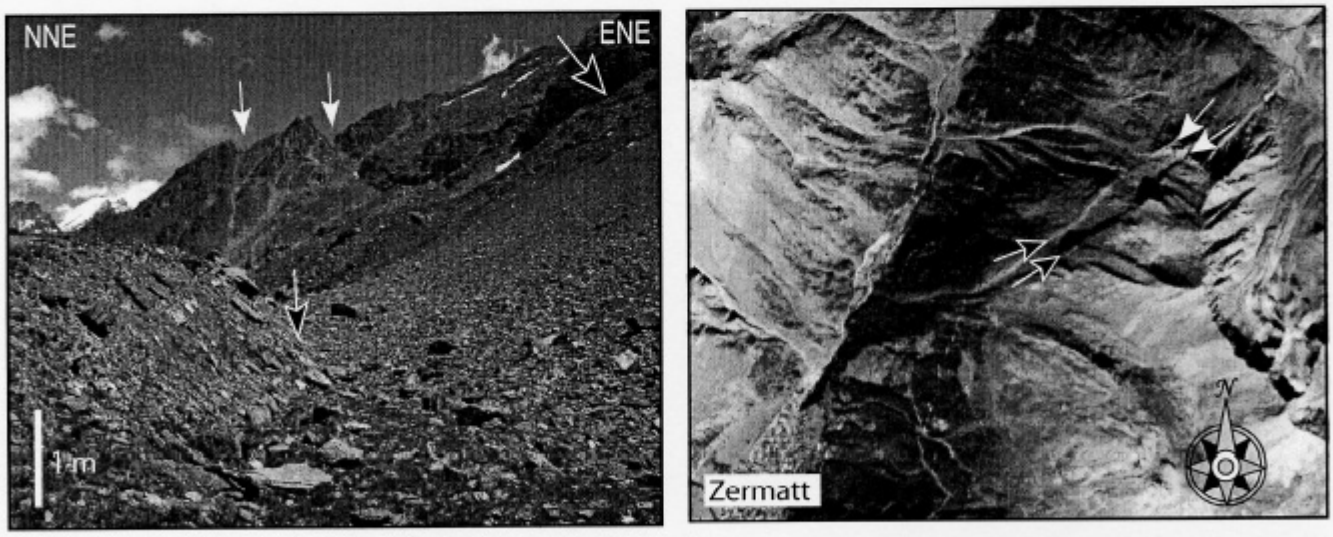

b

Fig. 2. Examples of brittle structures observed in the field.

Fig. 2a. Comparison between outcrop and remote sensing views of the Moiry fault. On the left, the outcrop seen from the point A (distance about 1 km). Several small normal faults are distinguishable (black arrows), conjugate with a larger fault, visible on the satellite image (white arrows). Note that the entire conjugate system is tilted about 30 degrees to the southwest.

Figure 2b: Comparison between field view and remote sensing view of a major fault system, in the vicinity of Zermatt. A) To the left, an outcrop, viewed from "inside" the fault system. B) To the right, the fault system seen in satellite image. Black arrows and white arrows show the same points on both pictures. At a larger scale, this fault zone runs beneath Zermatt.

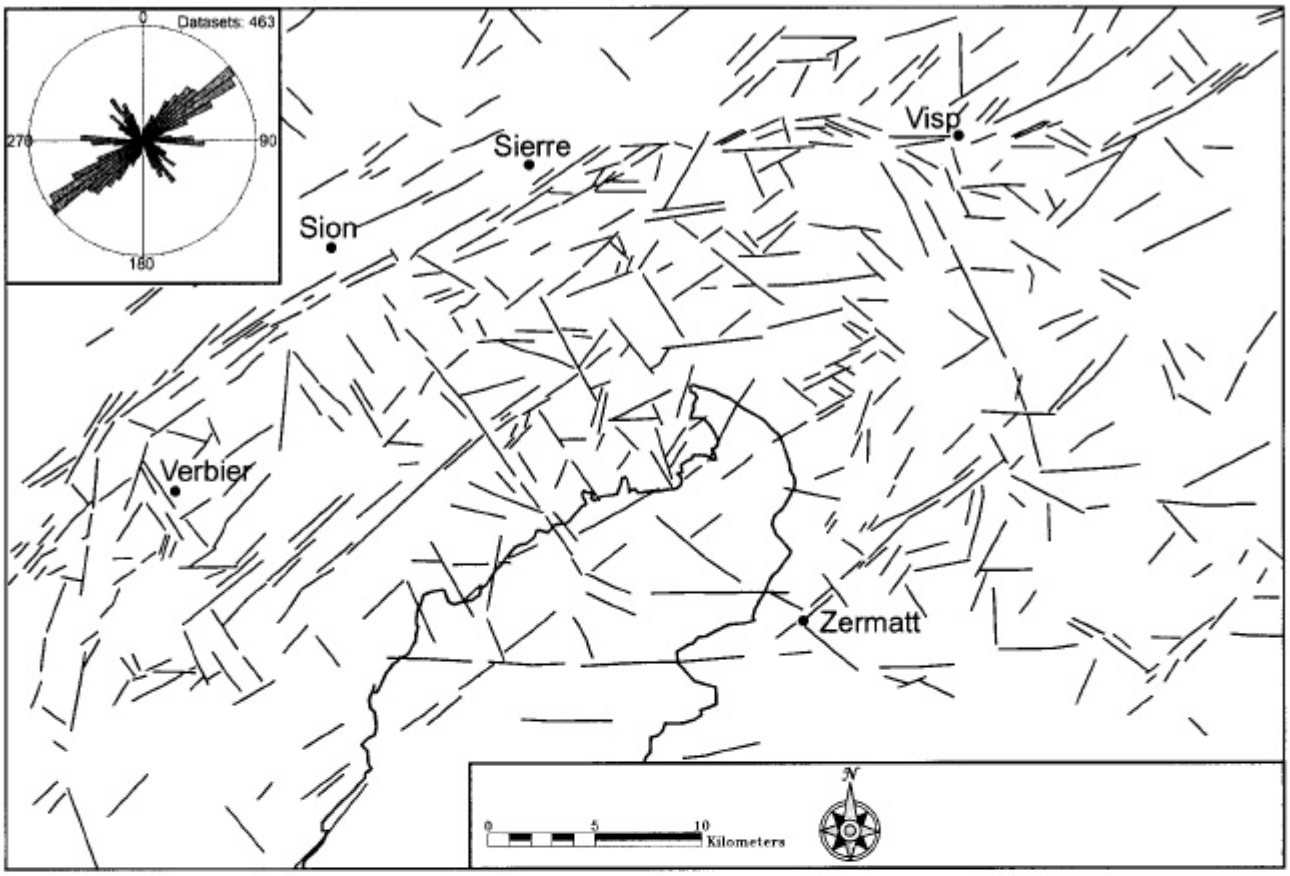

Fig. 3. Fault pattern of the Valais area, based on DEM analysis. Sion, Sierre and Visp, three towns in the Rhône valley are shown for reference. The "rose diagram" represents fault directions from the fault pattern. Three fault families (NW-SE, E-W and NE-SW) are easily distinguished. The contour of the Dent Blanche nappe is given for reference.

expression of easily removeable material such as schistes lustrés, calcschists and flyschs (Sion-Courmayeur zone, Versoyen unit), which have gentle to moderate dip to the SSE behind the External Crystalline Massif culminations (Aar massif). By coincidence, however, a Late Alpine normal/dextral strike-slip fault zone overprints the Basal Penninic Thrust along the Central Valais, adding to the structural complexity of this area (Burkhard 1986, 1988, Ménard 1988, Hubbard & Mancktelow 1992, Sartori 1993, Steck & Hunziker 1994). The existence of this Late Alpine, post nappe normal/dextral fault is not obvious, not least because the main branch of this fault zone is hidden beneath the fluvio-glacial quaternary sediments of the Rhône valley. Based on a marked difference in fission tracks apatite cooling ages on either side of the Rhône valley, a fairly recent, late Miocene age of faulting has been postulated (Soom 1990, Seward & Mancktelow 1994). Fairly high seismicity in the Central Valais area has been used as an argument for ongoing tectonic activity (Maurer et al. 1997, Deichmann et al. 2003).

To the west, the Basal Penninic Thrust turns around to a NNE-SSW orientation, bordering the ESE internal side of the Mont-Blanc massif. The Rhône fault zone does not follow the Basal Penninic Thurst, however, but cuts further downward into the footwall, following the Chamonix syncline between the Mont-Blanc and the Aiguilles Rouges massif (Burkhard 1988, Hubbard & Mancktelow 1992). It is described as transpressive dextral fault zone, the "Chamonix line" after (Gourlay 1984). Seismotectonics studies also show dextral focal mechanisms on a N30° oriented fault, close to the Chamonix line (Deichmann et al. 2003).

At the scale of the belt, the Simplon-Rhône-Chamonix line forms a large, slightly curved fault zone, changing its strike from NW-SE oriented to NE-SW, as well as its nature, being transtensive in the east and transpressive further westward.

The fault pattern we studied in this paper clearly crosscuts all the ductile compression-related structures and of nappe pile at the local and regional scales, although some faults may locally be guided by inherited nappe contacts. Thus, the brittle deformation clearly postdates the ductile deformations and nappe emplacement, and reflects the recent Alpine history (Neogene times).

3. Geometry of the late Alpine brittle deformation

A regional scale fault networks have been identified using a panchromatic IRS satellite image with a 6m-pixel resolution in combination with Digital Elevation Model (DEM) of 25m resolution (Swiss Topographic Survey). The satellite image and the DEM were examined with the help of the IDL/ENVI software package, using numerical filtering such as directional lightning, first and second derivative, and color coding of slope orientations. The filter were applied with several "kernel size" (the size of the sliding box within the computation is made) in order to highlight several wavelength structure. These numerical treatments highlight slope anomalies of only a few degrees, which could be manually drawn as lineaments. Those lineaments were systematically cross-checked with existing geologic and tectonic maps (Steck et al. 2000, Steck et al. 2001) and verified in the field (see examples in Fig. 2 a and 2 b), which justify their interpretation as brittle tectonic feature (faults). Our lineation map (Fig. 3) exhibits hectometric to kilometric lengths faults. Their geomorphic expression in the field varies from deep obvious gullies to subtle variations in gentle slopes. The linear alignment of such features crossing several lateral, southern side streams of the Rhône river is quite obvious on both the satellite image and the DEM. In total, we identified a set of about 500 faults, ranging from 400 m to 10 km in length. We decided to draw the observed faults without any interpolation (*i.e.* with a minimum subjective interpretation between several detected fault segments).

Three fault families have been distinguished (insert in Fig. 3).

A first fault family is oriented NE-SW and represents the main brittle tectonic feature of the studied area. The maximum density of this family is located close to the Rhône valley. The most prominent faults are located near Vercorin (black circle on Fig. 3), where terraces and inverse slopes of up to 100 m are observed. Road outcrops reveal the presence of thick series of cataclasites and fault gouges. The latter are often preferentially washed out along deep NE-SW striking gullies. Southward, at least five important, subparallel fault strands have been identified, within about ten kilometers.

A second fault family is oriented E-W. Two major fault zones are observable. To the north, an important fault zone shows thick cataclasite and fault gouge as well as important slope anomalies. This fault zone is the eastward continuation of the Rhône fault zone described above. To the south, close to the 4000m peaks, very long lineaments (over 40 km cumulated length) are parallel to the major Aosta-Ranzola fault system, which lies further to the South (Bistacchi et al. 2001). Other E-W faults have been observed in the central part of the southern Valais.

A third fault family is oriented NW-SE. The corresponding structures are more difficult to detect using the DEM, maybe due to specific relationships with the orographic scheme of the southern Valais (NW-SE oriented major valleys). Nevertheless, this fault family is revealed by our morphotectonics analysis, and is strongly developed on the outcrop scale. Faults of this family occur over the entire study area.

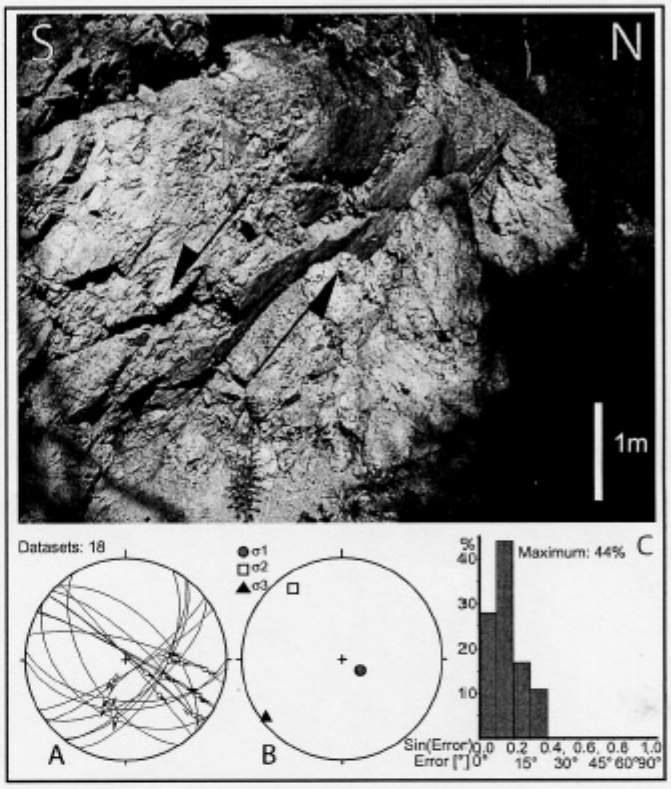

Fig. 4. Example of normal faults used in paleostress calculation from the Vercorin outcrop (black circle on Fig. 3).
At the top, a normal fault, very fresh and polished; A: 18 faults used for the paleostress tensor calculation, plotted on a Wulff stereogram, lower hemisphere; B: paleostress tensor (N50 direction of extension); C: misfit angle histogram.

These results are consistent with the remote sensing lineaments map by (Bistacchi et al. 2000) further to the south and complete them, providing a fine lineament map for the whole "Valais-Aosta valley" zone.

4. Paleostress analysis

Field measurements include a determination of the general fault orientation as well as a systematic collection of minor fault populations for the determination of paleostress axis directions by inversion methods (see example in Fig. 4). Paleostress analyses have been applied in the field wherever a sufficient number of striated faults could be measured. We used the "direct inversion method" of Angelier (1990) implemented in the "TectonicsFP" software (Sperner et al. 1993) for calculations and graphic outputs. About 1000 fault planes and their slickensides were measured at 56 sites covering the whole area of interest. Locally, two superimposed brittle deformation stages have been observed on fault planes, allowing the determination of two paleostress tensors. In this case, their relative

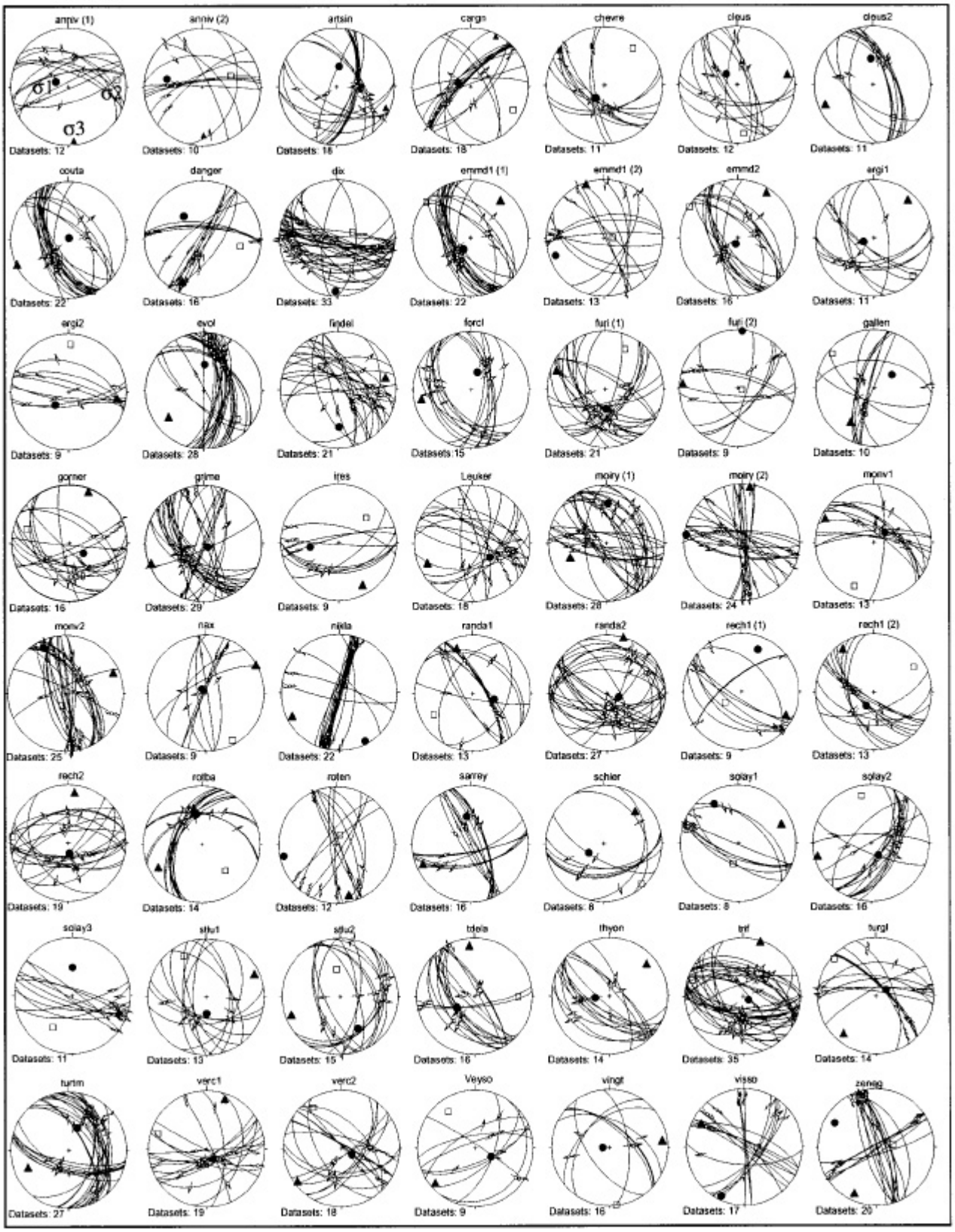

Fig. 5. Stereonets of the 56 paleostress tensors computed in this study (Wulff stereograms, lower hemisphere). Gray circles represents σ1 axis, white squares represents σ2 axis and black triangles represents σ3 axis. Faults and striae used for the calculation are also plotted.

Tab. 1. Parameters of the 56 paleostress tensors, with the location (x and y the swiss coordinate, z the altitude in meters), the σ1, σ2, and σ3 orientations (azimuth, plunge), and the Φ ratio. Also given are the number of faults used for the computation ("data" column), the quality criterion ("conf." column), and the average misfit angle ("var". column in degree °).

N∞	Site	x	y	z	s 1	s 2	s 3	F	data	conf.	var. (∞)
1	anniv (1)	609600	123550	1000	271 / 71	082 / 17	174 / 09	0,52	12	1	6
2	anniv (2)	609600	123550	1000	283 / 37	068 / 47	178 / 18	0,49	10	3	5,7
3	artsin	599100	107100	2960	008 / 61	207 / 27	113 / 08	0,47	18	1	11,5
4	cargn	609200	120000	1400	285 / 73	118 / 17	027 / 04	0,08	18	2	6,5
5	chevre	599400	96150	2870	214 / 69	038 / 21	307 / 01	0,2	11	2	5,5
6	cleus1	590900	106900	2100	315 / 69	172 / 17	079 / 12	0,06	12	2	2,9
7	cleus2	591300	106300	2200	355 / 53	148 / 33	247 / 13	0,32	11	1	3,2
8	couta	604000	103300	1910	026 / 87	154 / 02	244 / 02	0,22	22	1	9,4
9	danger	590950	96500	1700	320 / 48	101 / 35	206 / 20	0,95	16	1	6,7
10	dix	597500	104000	2000	182 / 09	069 / 67	271 / 21	0,97	33	2	7,3
11	emdd (1)	630800	119000	1380	210 / 71	309 / 03	040 / 19	0,06	22	2	4,8
12	emdd (2)	630800	119000	1380	250 / 12	088 / 78	341 / 03	0,24	13	3	7,8
13	emmd2	632500	12000	1080	202 / 81	303 / 02	033 / 08	0,07	16	1	7,6
14	ergi1	620700	127065	1080	250 / 74	134 / 07	042 / 14	0,4	11	2	5,3
15	ergi2	620549	126380	828	226 / 64	002 / 19	098 / 17	0,93	9	3	9,8
16	evole	605000	106200	1500	002 / 53	131 / 25	233 / 25	0,26	28	1	4,3
17	findel	626800	95600	2200	179 / 36	326 / 49	076 / 17	0,77	21	2	9,7
18	forcl	601300	97500	2800	020 /64	164 / 21	260 / 14	0,45	15	1	7,7
19	furi (1)	622700	94100	1860	178 / 63	026 / 25	291 / 11	0,08	21	1	6,3
20	furi (2)	622700	94100	1860	005 / 01	107 / 83	275 / 07	0,91	9	2	5
21	gallen	627050	99600	2300	053 / 59	309 / 08	215 / 30	0,79	9	2	4,3
22	gorner	626900	92500	3195	126 / 65	288 / 24	021 / 07	0,5	16	2	10
23	grime	609326	112032	1921	129 / 82	340 / 07	249 / 04	0,32	29	1	8,6
24	ires	584700	102300	1400	261 / 49	048 / 36	151 / 17	0,24	9	3	7,6
25	leuker	617000	129000	900	129 / 58	344 / 27	146 / 16	0,23	18	2	7
26	moiry (1)	610618	106618	2324	002 / 32	124 / 40	248 / 34	0,45	28	1	10,3
27	moiry (2)	610618	106618	2324	277 / 03	151 / 84	008 / 04	0,63	24	3	16,5
28	monv1	593800	92500	2100	048 / 69	204 / 19	296 / 08	0,11	13	3	6,3
29	monv2	592400	94700	1820	334 / 13	196 / 72	064 / 11	0,49	25	1	9,6
30	nax	601550	120950	1020	318 / 82	151 / 08	061 / 02	0,22	9	3	6,1
31	nikla	626900	112400	1500	152 / 05	034 / 79	243 / 10	0,49	22	2	12,5
32	randa1	625950	103950	1600	105 / 59	241 / 24	340 / 19	0,78	13	3	13,6
33	randa2	624900	103600	2090	107 / 73	287 / 17	017 / 00	0,13	27	1	7,5
34	rech1 (1)	604600	121500	1010	022 / 23	326 / 62	118 / 14	0,78	9	2	2
35	rech1 (2)	604600	121500	1010	209 / 68	058 / 19	325 / 10	0,13	13	2	5
36	rech2	604300	121000	1200	173 / 76	276 / 03	007 / 14	0,03	19	1	8,9
37	rotba	629550	101500	2550	350 / 46	138 / 39	242 / 16	0,04	14	2	2,4
38	roten	625400	92700	2820	258 / 08	019 / 75	167 / 12	0,75	12	2	5,5
39	sarray	586050	100900	1129	353 / 51	148 / 37	247 / 12	0,87	16	1	4,8
40	schler	587000	101900	2000	239 / 65	137 / 05	045 / 24	0,16	8	3	3,8
41	solay1	608400	101400	1800	329 / 22	195 / 60	067 / 19	0,06	8	3	6,2
42	solay2	607650	102400	1700	150 / 71	349 / 18	257 / 06	0,17	16	2	8,6
43	solay3	607300	102600	1700	000 / 50	212 / 36	110 / 16	0,98	11	3	3,5
44	stlu1	611900	119850	1720	178 / 67	331 / 21	065 / 10	0,23	13	1	3,3
45	stlu2	612600	118400	1580	151 / 37	353 / 51	249 / 11	0,6	15	2	6,3
46	tdela	594800	111600	2160	238 / 61	091 / 25	354 / 14	0,08	16	3	3,9
47	thyon	594700	114000	2160	262 / 70	142 / 10	049 / 17	0,29	14	2	6,3
48	trift	623300	96900	1800	123 / 81	288 / 09	018 / 02	0,33	35	1	8,7
49	turgl	620863	110796	2728	049 / 89	175 / 01	265 / 01	0,83	15	2	10,4
50	turtm	619441	113221	2150	022 / 57	147 / 21	247 / 25	0,24	27	1	7,5
51	verc1	608193	122849	1151	147 / 73	287 / 13	020 / 11	0,01	19	2	11,4
52	verc2	608000	121700	1350	122 / 73	325 / 16	233 / 06	0,3	18	2	10,6
53	veyso	591700	115700	1000	118 / 65	323 / 23	229 / 09	0,14	9	2	3,8
54	vingt	596600	102500	2380	271 / 81	173 / 01	083 / 09	0,57	16	1	3,8
55	visso	610900	120200	1100	205 / 08	091 / 71	298 / 17	0,85	17	3	5,6
56	zeneg	633245	125295	1350	300 / 19	082 / 67	206 / 13	0,59	20	3	6,2

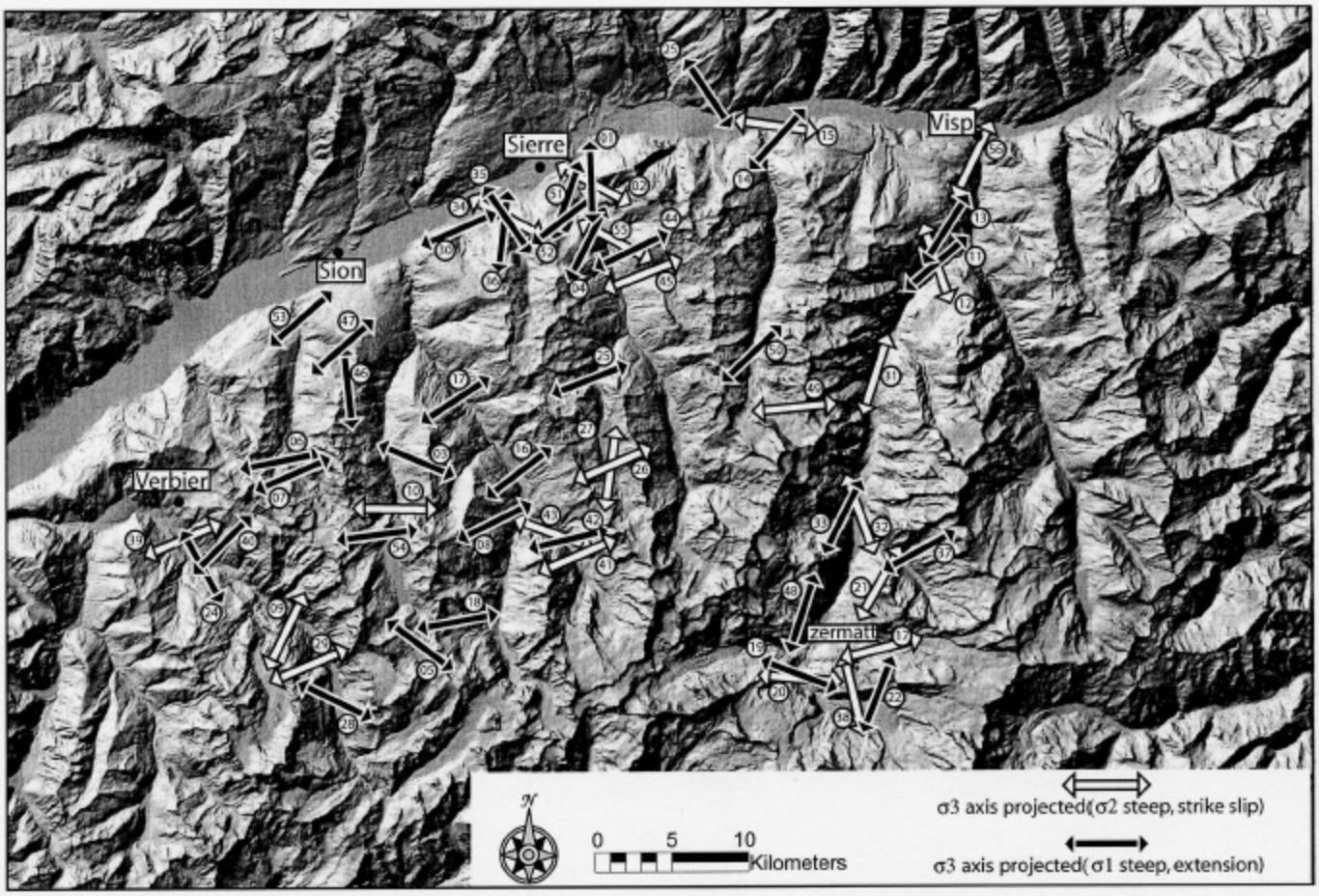

Fig. 6. Paleostress direction map, with σ3 horizontal axis projected; white arrows for strike-slip tensors (subhorizontal σ1), black arrows for extensional tensors (subvertical σ1).

chronology has been deduced from slickensides crosscutting relationships. For each paleostress tensor, we calculated the directions of the major, intermediate and minor stress axis (σ1, σ2 and σ3 respectively), the ellipsoid form parameter $\Phi = (\sigma2-\sigma3)/(\sigma1-\sigma3)$ and the average misfit angle α, which is the angle between the computed optimum stria and the measured stria for each fault/stria pair. The angle α provides a rapid estimation of the quality and coherence of the measured fault population. Individual faults with angles too high ($\alpha>30°$) were discarded from the final calculation in order to maintain a geological and mechanical coherency (note that they only represented around 10% of the measurements).

The quality of the tensors is estimated *a priori* on the basis of four criteria:

- The number of faults in the computation, and their spatial coverage. Sites with less than 8 faults were not considered.
- The coherency between paleostress inversion and the geometrical solution obtained from the right diedra method (Angelier & Mechler 1977). The results need to be comparable.
- The stability of the computation with respect to particular faults. Some faults create large variation of the axis direction when added (or removed) from the dataset. In this case, the tensor has a lower quality criterion.
- The average misfit angle (α).

Three classes of quality for the stress tensors were defined, from 1 (excellent) to 3 (poor). The results of this analysis is a database of 56 paleostress tensors covering the whole area (Fig. 5, Table 1).

The paleostress results are presented in map form, plotted onto the DEM of the South Valais (Fig. 6). A majority of our stress tensors are extensive (*i.e.* σ1 steep) with a regionally consistent ENE-WSW (N65°) direction of extension. About 30% of the stress tensors are transcurrent (*i.e.* σ2 steep), with about the same σ3 direction. Based on striae crosscutting relationships, the strike-slip deformation seems to be older than the extensional deformation. The σ3 direction in the entire studied area is stable, and no significant change is observed between the strike-slip and extensional tensors (Fig. 7). Additional information about the shape of the paleostress ellipsoid

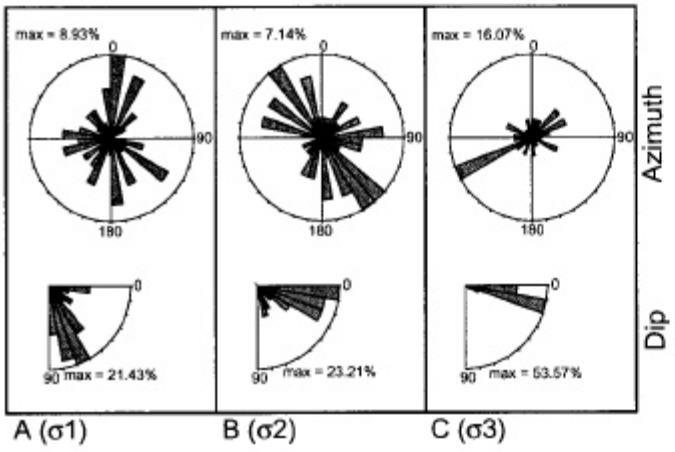

Fig. 7. Rose diagram showing azimuth (top) and dip (bottom) of σ1 (A), σ2 (B) and σ3 (C) for the 56 calculated tensors.

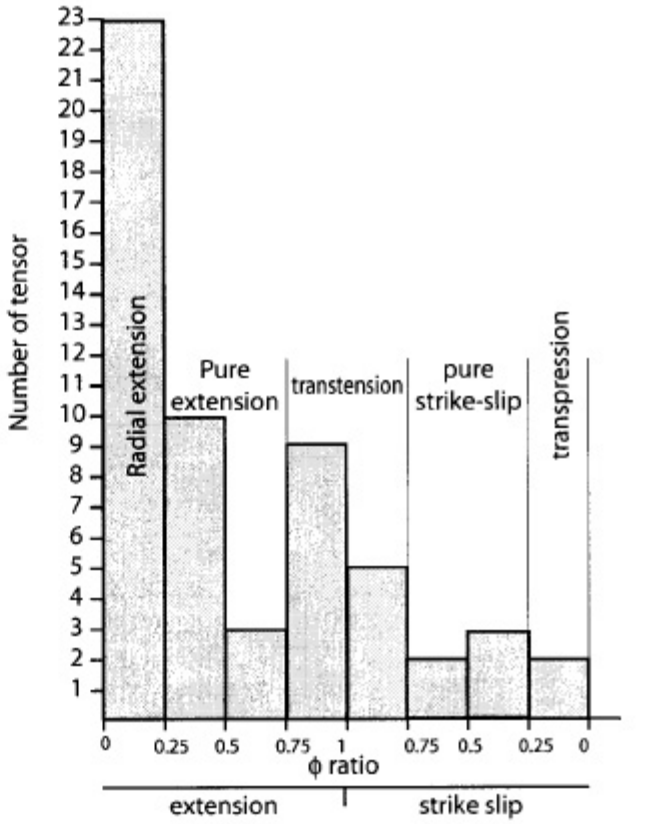

Fig. 8. Histogram showing the number of tensors *versus* Φ ratio. This histogram is split into two categories, from Φ=0 to Φ=1 for extensional tensors (to the left), Φ=1 to Φ=0 for strike-slip tensors (to the right). From left to right, we observe a continuum from radial extension, pure extension, transtension, strike-slip and transpression.

is contained in the Φ ratio, a convenient measure of the relative magnitude of σ1, σ2 and σ3. In the case of extensional tensors (σ1 steep), a low Φ ratio implies similar σ2 and σ3, indicating radial extension. A high Φ ratio implies similar σ1 and σ2, which indicates transtension wheras an intermediate Φ ratio indicates a pure extensional paleostress tensor. For strike-slip tensors (σ2 steep), a low Φ ratio (similar σ3 and σ2) implies a transpressional stress field, a medium Φ ratio implies pure strike-slip and a high Φ ratio implies transtension. Note that the majority of our strike-slip tensors have a high Φ ratio, and thus correspond to transtension. Using this approach, we have analyzed our database in terms of Φ ratio, mixing extensional and strike-slip tensors. We have classified the tensors within three classes, $\Phi<0.25$, $0.25<\Phi<0.75$ and $\Phi>0.75$ despite the fact that our tensors probably belong to a bimodal distribution with respect to their Φ ratio (Fig. 8).

The extensive tensors with $0.25<\Phi<0.75$ (Fig. 9 a) show consistent WSW-ENE direction of extension for 12 paleostress tensors.

The 22 extensive tensors with $\Phi<0.25$ (Fig. 9 b) show almost the same direction as the previous ones. Some of them exhibit a NW-SE direction of extension, which could be explained by a permutation between σ2 and σ3. Despite a fairly consistent σ3 orientation, an important part of the paleostress field in the South Valais seems to correspond to radial extension.

A population of 13 transtensional tensors with $\Phi>0.75$ shows a fairly consistent direction of σ3 (NNE to ENE) in close agreement with another 9 transcurrents tensors (Fig. 9 c). Some of these tensors have quite different directions of σ3, but most of them have a poor quality criterion.

In summary, we have analyzed our fault database in order to constrain the brittle paleostress field in the South Valais. The classical analysis (strike slip versus extensional tensors, depending on the stress ellipsoid orientation) shows that the stress tensor is mainly extensional, with a WSW-ENE orientation for σ3 (N65°). The use of Φ ratios to characterize the shape of the paleostress ellipsoid allowed us to sort the paleostress tensors into several classes and to analyze the database in finer detail. In particular, some of the extensive tensors are rather close to strike-slip tensors, reflecting a transtensive paleostress field. We also sorted our database using the quality parameter. Choosing only the best tensors (with quality criterion 1 or 2, see Fig. 10) improves the coherency of the dataset, and of the paleostress field. Overall, the σ3 orientation WSW-ENE appears to be very stable and robust across the whole area.

Discussion and conclusion

This study highlights a generalized brittle extensional paleostress field in the southern Valais, by means of a well established inversion method. This study also confirms the large scale brittle extension already highlighted by (Bistacchi et al. 2000) and improve the paleostress field framework. We found mainly normal faulting, as well as some older sets of strike-slip faults. The bimodal distribution of the Φ ratio, coupled with field observations and paleostress tensor calculations reveals

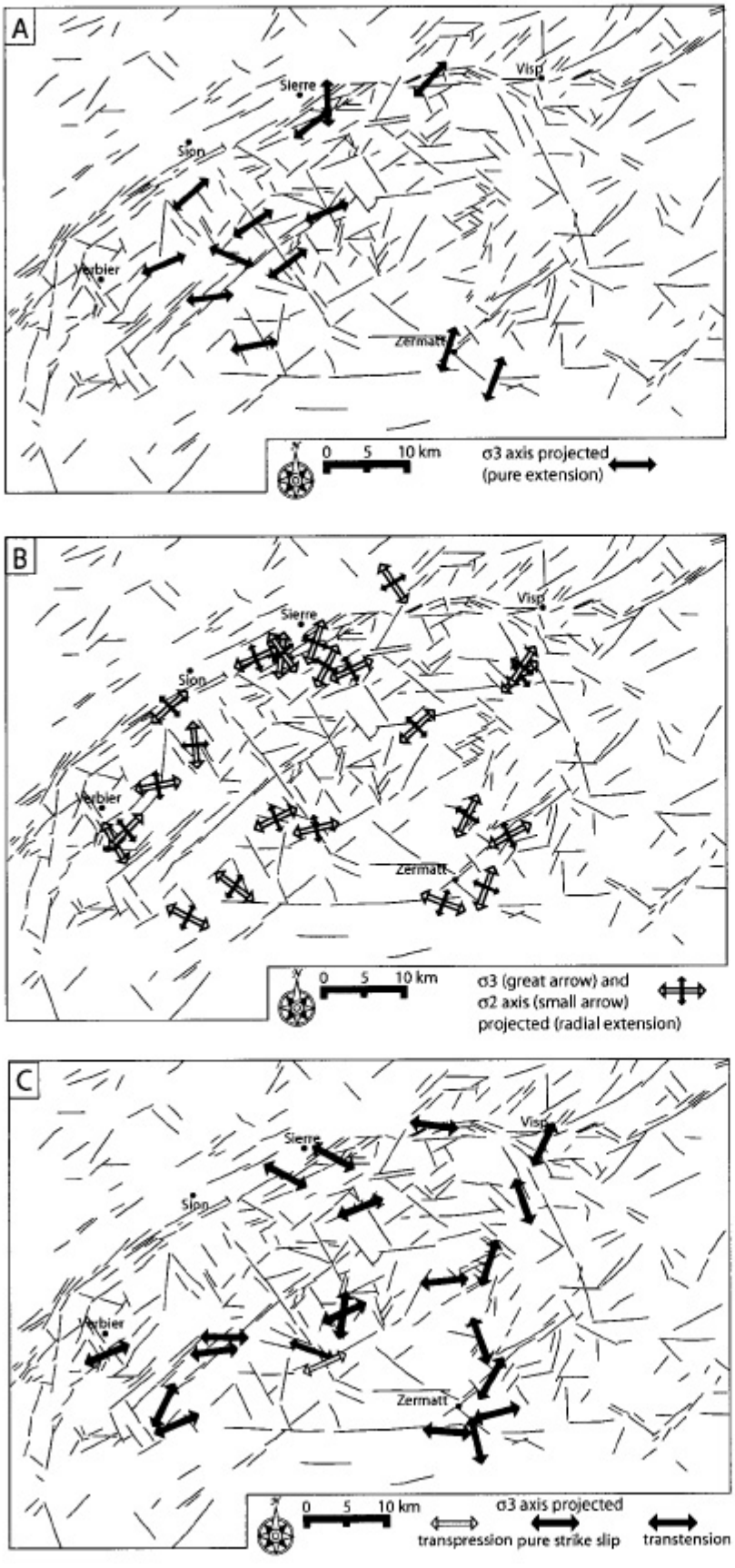

Fig. 9. Three maps showing σ3 orientations (projected subhorizontal axis) for medium (Fig. 9a), low (Fig. 9b) and high (Fig. 9c) Φ ratio paleostress tensors respectively.

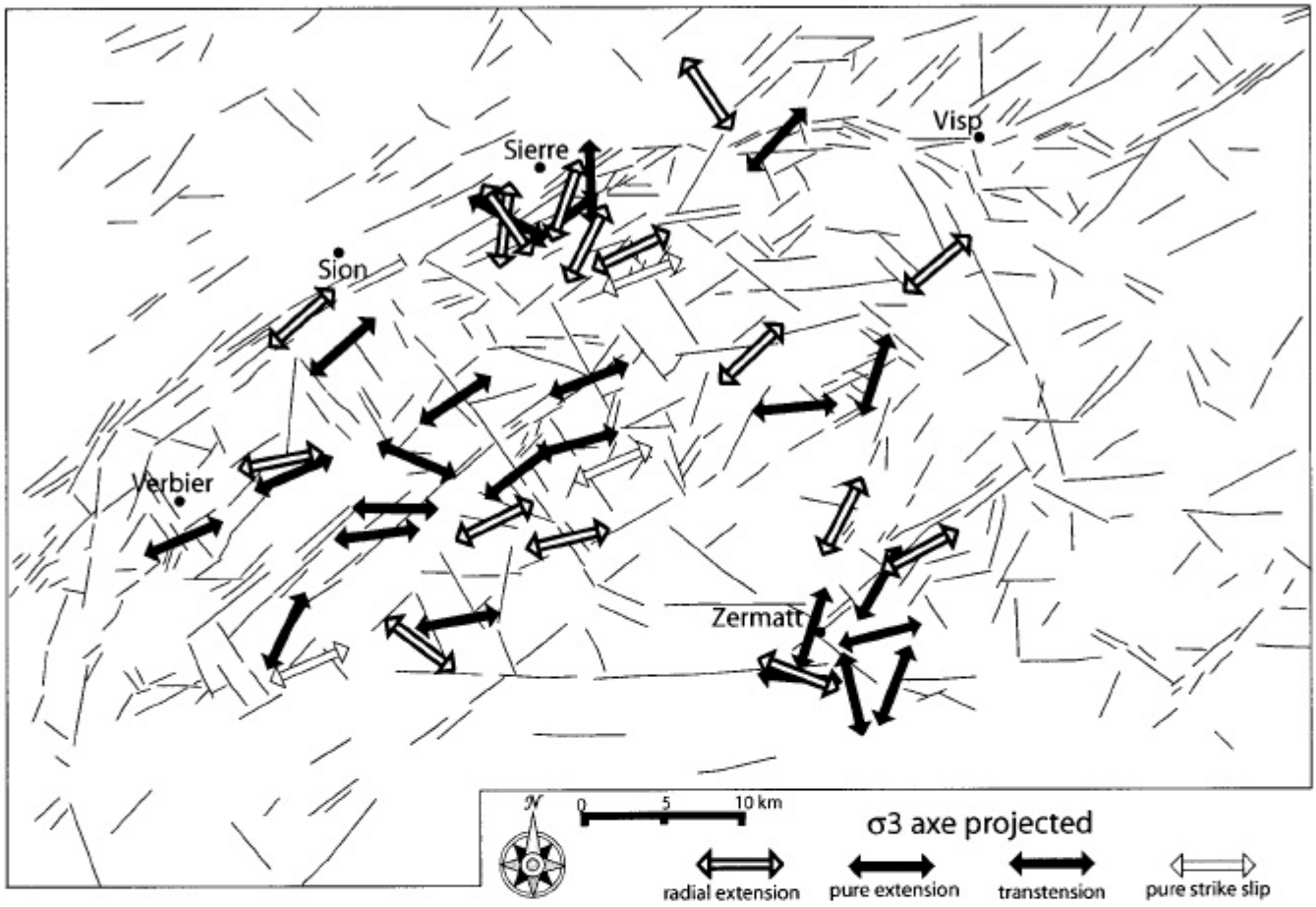

Fig. 10. σ3 axis projected for the best quality tensors (quality criterion = 1 or 2). Note that the overall coherency of the whole dataset is highly improved, with a general direction of σ3 close to N65.

the presence of at least two populations of paleostress tensors. The first one corresponds to a transcurrent/transtensive paleostress field, expressed as strike-slip faulting and oblique normal faulting. The second one corresponds to an extensional paleostress field, with a NE-SW (N65°) oriented σ3, expressed as important normal faulting. The relative chronology is determined from cross cutting relationships between superimposed slikensides, consistently observed on several outcrops.

A statistical analysis of the paleostress axis (σ1, σ2 and σ3, see the three rose-diagrams of Fig. 7) underlines the consistency of the horizontal σ3 axis oriented ENE-WSW, dipping less than 15°. In contrast, the maximum compressive stress σ1 is near vertical, with a dip of more than 70° for the second generation. The common σ3 orientation associated with many curved slickensides observed on the faults planes led us to propose a progressive transition from the transtensional stress field to the extensional stress field. This can be explained with a σ1/σ2 permutation, without any change in the σ3 direction.

Compared to recent seismotectonic studies (Maurer et al. 1997, Kastrup et al. in press, Delacou et al. submitted), we can establish a more complete chronology for the stress field in the southern Valais. The focal plane solutions for the southern Valais area show a globally N-S T-axis ("tension" axis). The associated current stress field, computed by inversion of the focal solution is extensional, with a σ3 N-S.

In summary, we distinguish three successive orientations of (paleo-)stresses, probably within a continuous evolution.

First, a transtensive stress field, with σ3 oriented in a N65° direction and associated with σ1 or σ2 oriented in a N155 direction. This stress field is responsible for dextral movement along the ENE-WSW to E-W oriented Rhône fault zone in good agreement with previous studies (Burkhard 1986, 1988, Hubbard & Mancktelow 1992, Mancktelow 1992, Sartori 1993).

Second, a progressive permutation of σ1 and σ2 stress axis leads to an extensional regime. This stress field induces pure extension on NW-SE oriented faults. The local variation of the relative σ1/σ2 value could explain the progressive passage from the first stage to the second stage (σ1/σ2 permutation around the σ3 axis). Note that the σ3 direction remains constantly NE-SW oriented. Most of the paleostress tensors determined have a similar relatively low σ2/σ3 value (*i.e.* a low Φ

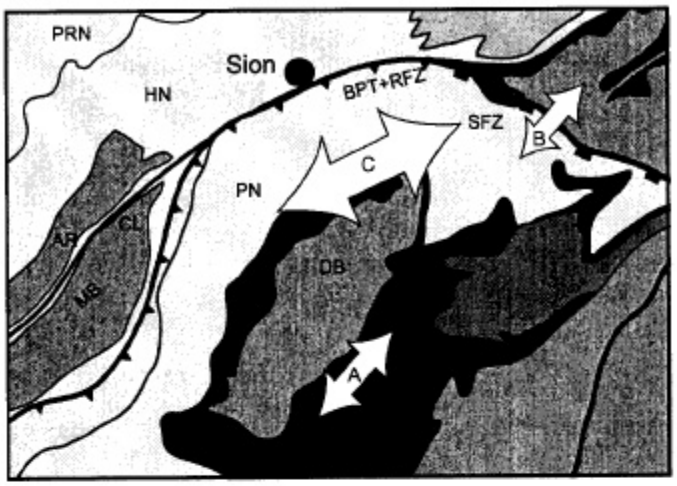

Fig. 11. Synthetic view of the post-nappe brittle deformation in the "Simplon-Valais-Aosta" area after (Bistacchi & Massironi 2000) (A), (Mancktelow 1992) and (Grosjean et al. in press) (B) and this paper (C). Legend for geologic structures as in Fig. 1.

ratio), inducing a radial extension of the southern Valais area, although the σ3 axis remains constantly oriented in the N65° direction.

Third, seismotectonic studies indicate a present day N-S pure extension, most probably responsible for extensional re(?)-activation of the EW oriented fault family. Some of our computed paleostress tensors are in good agreement with this last stress field, especially close to the Rhône valley and in the Zermatt valley (sites N° 01, 13, 33, 36, and 48, for the most constrained tensors).

The overall stress fields we have computed in the southern Valais are in good agreement with NE-SW extension observed in the Simplon Fault Zone, (Mancktelow 1992, Grosjean et al. in press). Our study especially emphasizes the regional scale of orogen-parallel extension, as it is now described in the Simplon Fault Zone, in the whole southern Valais area, and in the Val d'Aoste area further to the South (Bistacchi & Massironi 2000). Accordingly, we can propose a generalized orogen-parallel extension homogeneous in the entire "Simplon-Valais-Aosta" area.

Neogene and ongoing extensional tectonics in the western and particularly northwestern Alps remains to be explained in terms of a unifying geodynamic process. A major question concerns the relationship between the orogen-parallel extension in the Simplon-Valais-Aosta area and the radial brittle extension described in the southwestern Alps, especially in the Briançon area (Sue & Tricart 2002). Moreover, the link with the ongoing large scale radial extension (Sue et al. 1999, Kastrup et al. in press, Delacou et al. submitted) remains to be clarified. Local kinematics or dynamic interpretations, such as regional southwestward extrusion phenomenon in the northwestern Alps (Hubbard & Mancktelow 1992, Bistacchi & Massironi 2000), counterclockwise rotation in the belt (Ménard 1988, Vialon et al. 1989, Thomas et al. 1999, Collombet et al. 2002), associated with extrusion of the Lepontine dome (Steck & Hunziker 1994, Frisch et al. 2000, Wawrzyniec et al. 2001) and/or buoyancy forces in the root of the belt may account for this extension. Recent geodetic studies (Calais et al. 2002, Oldow et al. 2002) suggest no (or very low) shortening accommodated in the western Alps while the seismotectonic extension is radial to the bend. According to this, the present dynamic of the arc seems to be different to the Miocene dynamic.

Acknowledgements

This work was supported by the Neuchâtel University and by the Swiss National Science Found (grant # 21-61684.00). We thank N.S. Mancktelow, M. Massironi and J. Remane for constructive reviews and comments. We are grateful to M. Sartori and P. Tricart for fruitful discussions. We wish to thank L. Bichsel, B&M. Dufour, N. Vouillamoz and Luna for their helpful participation in field work. We are also grateful to the persons who welcome us in the Valais region during field work.

REFERENCES:

ALBARELLO, D., MANTOVANI, E., BABBUCCI, D. & TAMBURELLI, C. 1995: Africa-Eurasia Kinematics – Main Constraints and Uncertainties. Tectonophysics 243(1–2), 25–36.

ANGELIER, J. 1990: Inversion of field data in fault tectonics to obtain the regional stress – A new rapid direct inversion method by analytical means. Geophys. J. Int. 103, 363–376.

ANGELIER, J. & MECHLER, P. 1977: Sur une méthode graphique de recherche des contraintes principales également utilisable en tectonique et en sismologie: la méthode des dièdres droits. Bull. Soc. Géol. France 7(XIX), 1309–1318.

ARGUS, D. F., GORDON, R. G., DEMETS, C. & STEIN, S. 1989: Closure of the Africa-Eurasia-north America plate motion circuit and tectonics of the Gloria fault. J. Geophys. Res. 94, 5585–5602.

BISTACCHI, A. & MASSIRONI, M. 2000: Post-nappe brittle tectonics and kinematic evolution of the north-western Alps: an integrated approach. Tectonophysics 327(3–4), 267–292.

BISTACCHI, A., EVA, E., MASSIRONI, M. & SOLARINO, S. 2000: Miocene to Present kinematics of the NW-Alps: evidences from remote sensing, structural analysis, seismotectonics and thermochronology. J. Geodyn. 30, 205–228.

BISTACCHI, A., DAL PIAZ, G. V., MASSIRONI, M., ZATTIN, M. & BALESTRIERI, M. L. 2001: The Aosta-Ranzola extensional fault system and Oligocene-Present evolution of the Austroalpine-Penninic wedge in the northwestern Alps. Int. J. Earth Sci. 90(3), 654–667.

BURKHARD, M. 1986: Déformation des calcaires de l'Helvétique de la Suisse occidentale (Phénomènes, mécanismes et interprétations tectoniques). Rev. Géogr. Phys. Géol. Dyn. 27(5), 281–301.

BURKHARD, M. 1988: L'helvetique de la bordure occidentale du massif de l'Aar (évolution tectonique et métamorphique). Eclogae Geol. Helv. 81, 63–114.

CALAIS, E., GALISSON, L., STEPHAN, J. F., DELTEIL, J., DEVERCHERE, J., LARROQUE, C., DE LEPINAY, B. M., POPOFF, M. & SOSSON, M. 2000: Crustal strain in the Southern Alps, France, 1948–1998. Tectonophysics 319(1), 1–17.

CALAIS, E., NOCQUET, J. M., JOUANNE, F. & TARDY, M. 2002: Current strain regime in the Western Alps from continuous Global Positioning System measurements, 1996–2001. Geology 30, 651–654.

CHOUKROUNE, P., BALLÈVRE, M., COBBOLD, P., GAUTIER, Y., MERLE, O. & VUICHARD, J. P. 1986: Deformation and motion in the western alpine arc. Tectonics 5(2), 215–226.

COLLOMBET, M., THOMAS, J., C., CHAUVIN, A., TRICART, P., BOULLIN, J. P. & GRATIER., J. P. 2002: Counterclockwise rotation of the western Alps since the Oligocene: New insights from paleomagnetic data. Tectonics 21, 352–366.

CRÉTAUX, J.-F., SOUDARIN, L., CAZENAVE, A. & BOUILLÉ, F. 1998: Present-day tectonic plate motions and crustal deformations from the DORIS space system. J. Geophys. Res. 103, 30167–30181.

DEICHMANN, N., BAER, M., BRAUNMILLER, J., BALLARIN DOLFIN, D., BAY, F., BERNARDI, F., DELOUIS, B., FÄH, D., GERSTENBERGER, M., GIARDINI, D., HUBER, S., KRADOLFER, M., MARAINI, S., OPRSAL, I., SCHIBLER, R., SCHLER, T., SELLAMI, S., STEIMEN, S. WIEMER, S., WÖSSNER, J. & WYSS, A. 2003: Earthquake in switzerland and surrounding region during 2002. Eclogae Geol. Helv. 96, 313–324.

DELACOU, B., SUE, C., CHAMPAGNAC, J. D. & BURKHARD, M. submitted: Present-day geodynamics in the bend of the western and central Alps as constrained by earthquake analysis. Geophys. J. Int.

DEMETS, C., GORDON, R. G., ARGUS, D. F. & STEIN, S. 1990: Current plate motions. Geophys. J. Int. 101, 425–478.

DEMETS, C., GORDON, R. G., ARGUS, D. F. & STEIN, S. 1994: Effect of recent revisions to the geomagnetic reversal time scale on estimates of current plate motions. Geophys. Res. Lett. 21, 2191–2194.

DESMONS, J., APRAHAMIAN, J., COMPAGNONI, R., CORTESOGNO, L., FREY, M., GAGGERO, L., DALLAGIOVANNA, G., SENO, S. & RADELLI, L. 1999: Alpine metamorphismof the western Alps: middle to high P/T metamorphism. Schweiz. Mineral. Petrogr. Mitt. 79, 89–110.

ESCHER, A., HUNZIKER, J., MASSON, H., SARTORI, M. & STECK, A. 1997: Geologic framework and structural evolution of the western Swiss-Italian Alps. In: O.A. PFIFFNER, P. LEHNER, P.Z. HEITZMAN, S. MUELLER AND A. STECK (Eds.), Deep structure of the Swiss Alps – Results from NRP 20. Birkhäuser AG. Basel., 205–222.

FREY, N., DESMONS, J. & NEUBAUER, F. 1999: Metamorphic maps of the Alps. Schweiz. Mineral. Petrogr. Mitt. 79.

FRISCH, W., SZEKELY, B., KUHLEMANN, J. & DUNKL, I. 2000: Geomorphological evolution of the Eastern Alps in response to Miocene tectonics. Z. Geomorphologie 44(1), 103–138.

GOURLAY, P. 1984: La déformation alpine des massifs cristalins externes (Mont-Blanc, Aiguilles-Rouges, Belledonne) et celle de leur couverture mésozoïque (Alpes occidentales).PhD Thesis, Université Pierre et Marie Curie, Paris 6.

GRASEMANN, B. & MANCKTELOW, N. S. 1993: Two-dimensional thermal modelling of normal faulting: the Simplon Fault Zone, Central Alps, Switzerland. Tectonophysics 225(155–165).

GROSJEAN, G., SUE, C. & BURKHARD, M. in press: Late Neogene brittle extension in the vicinity of the Simplon fault zone, central Alps, Switzerland. Eclogae Geol. Helv.

HUBBARD, M. & MANCKTELOW, N. S. 1992: Lateral displacement during Neogene convergence in the western and central Alps. Geology 20, 943–946.

HUNZIKER, J., DESMONS, J. & HURFORD, A. J. 1992: Thirty-two years of geochronological work in the Central and Western Alps: a review on seven maps. Mém. géol. Lausanne 13.

KASTRUP, U., ZOBACK, M. L., DEICHMANN, N., EVANS, K. & GIARDINI, D. in press: Stress field variations in the Swiss Alps and the northern Alpine foreland derived from inversion of fault plane solutions. J. Geophys. Res.

KREEMER, C. & HOLT, W. E. 2001: A no-net-rotation model of present day surface motion. Geophys. Res. Lett. 28, 4407–4410.

LE PICHON, X., BERGERAT, F. & ROULET, M. J. 1988: Plate kinematics and tectonics leadingto the alpine belt formation; a new analysis. Geol. Soc. Amer. Bull. 218, 111–131.

MANCEL, P. & MERLE, O. 1987: Kinematics of the northernpart of the Simplon line (central Alps). Tectonophysics 135, 265–275.

MANCKTELOW, N. S. 1985: The Simplon line: a major displacement zone in the western Lepontine Alps. Eclogae Geol. Helv. 78, 73–96.

– 1990: The Simplon fault zone. Breit. Geol. Karte Schweiz (NF) 163, 74 pp.

– 1992: Neogene lateral extension during convergence in the Central Alps: Evidence interrelated faulting and backfolding around the Simplonpass (Switzerland). Tectonophysics 215, 295–317.

MASSIRONI, M., BAGGIO, P., DAL PIAZ, G. V. & LOIZZO, R. 1997: Brittle tectonics in Northwestern Alps: remote sensing applications. In: CECCHI, G., ENGMAN E.T., ZILIOLI, E. (eds.), Earth Surface Remote Sensing. EUROPTO Series. 3322, 329–339.

MAURER, H., BURKHARD, M., DEICHMANN, N. & GREEN, G. 1997: Active tectonism in the central Alps: Contrasting stress regimes north and south of the Rhone Valley. Terra Nova 9, 91–94.

MÉNARD, G. 1988: Structure et cinématique d'une chaîne de collision: Les Alpes occidentales et centrales. Thèse de Doctorat d'état, Université Joseph Fourier. Grenoble.

MOSAR, J. 1999: Present-day and future tectonic underplating in the western Swiss Alps: reconciliation of basement/wrench-faulting and decollement folding of the Jura and Molasse basin in the Alpine foreland. Earth and planet. Sci. Lett. 173(3), 143–155.

NOCQUET, J.-M. 2002: Mesure de la déformation crustale en Europe occidentale par Géodésie spatiale.Thèse de doctorat, Université de Nice.307pp., Nice.

OLDOW, J. S., FERRANTI, L., LEWIS, D. S., CAMPBELL, J. K., D. A. B, R. C., PAPPONE, G., CARMIGNANI, L., CONTI, P. & AIKEN, C. L. V. 2002: Active fragmentation of Adria, the north African promontory, central Mediterranean orogen. Geology 30, 779–782.

RATSCHBACHER, L., FRISCH, W., NEUBAUER, F., SCMID, S. M. & NEUGEBAUER, J. 1989: Extension in compressional orogenic belts: The eastern Alps. Geology 17, 404–407.

SARTORI, M. 1993: Une carte des décrochements dans la vallée du Rhône. In: N. Mancktelow (eds), Schweizer TektonikerTreffen. Lecture Abstracts, Zürich.

SELVERSTONE, S. M. 1988: Evidences for East-West crustal extension in the eastern Alps: implication for the unroofing history of the Tauern window. Tectonics 7, 87–105.

SEWARD, D. & MANCKTELOW, N. S. 1994: Neogene kinematics of the central and western Alps: Evidence from fission-track dating. Geology 22, 803–806.

SOOM, M. A. 1990: Abkülungs und Hebungsgeschichte der Extern Massive und der Penninischen Decken beidseits des Simplon-Rhône-Linie seit dem Oligozän: Spaltspurdatierungenan Apatit/Zircon und K-Ar Datierungenan Biotit/Muscovit (Westlische Zentralalpen). PhD Thesis Bern Univ., 120p.

SPERNER, B., OTT, R. & RATSCHBACHER, L. 1993: Fault-striae analysis: a turbo pascal program package for graphical presentation and reduced stress-tensor calculation. Computers & Geosciences 19(9), 1361–1388.

STECK, A. 1984: Structure de déformations tertiaires dans les Alpes centrales (transversale Aar-Simplon-Ossola). Eclogae Geol. Helv. 77, 55–100.

STECK, A. & HUNZIKER, J. 1994: The tertiary structure and thermal evolution of the central Alps – compressional and extensional structures in an orogenic belt. Tectonophysics 238, 229–254.

STECK, A., EPARD, J. L., ESCHER, A., MARCHANT, R. & MASSON, F. 1997: Geological interpretation of the seismic profiles through western Switzerland: Rawil (W1), Val d'Annivier (W2), Mattertal (W3), Zmutt-Zermatt-Findelen (W4), and Val de Bagnes (W5). In: O.A. Pfiffner, P. Lehner, P.Z. Heitzman, S. Mueller and A. Steck (Eds.), Deep structure of the Swiss Alps – Results from NRP 20. Birkhäuser AG. Basel.

STECK, A., BIGIOGGERO, B., DAL PIAZ, G., ESCHER, A., MARTINOTTI, G. & MASSON, H. 2000: Carte géologique des Alpes de Suisse occidentale, 1/100000. Carte géologique spéciale N° 123. Serv. Hydrol. géol. natl. (Berne).

STECK, A., EPARD, J. L., ESCHER, A., GOUFFON, Y. & MASSON, H. 2001: Carte géologique des Alpes de Suisse occidentale, 1/100000, notice explicative. In: Carte géologique spéciale N° 123. Office féd. Eaux Géologie (Berne).

SUE, C. 1998: Dynamique actuelle et récente des Alpes occidentales internes-Approche structurale et sismologique. PhD Thesis, Université Joseph Fourier. 299p., Grenoble.

SUE, C. & TRICART, P. 1999: Late Alpine brittle extension above the Frontal Pennine Thrust near Briancon, Western Alps. Eclogae Geol. Helv. 92(2), 171–181.

– 2002: Late-Alpine syncollisional extension in the core of the Western Alps inferred from faulting analysis. J. geol. soc. (London) 159, 61–70.

– in press: Neogene to current normal faulting in the inner western Alps: a major evolution of the late alpine tectonics. Tectonics.

SUE, C., THOUVENOT, F., FRECHET, J. & TRICART, P. 1999: Widespread extension in the core of the western Alps revealed by earthquake analysis. J. geophys. Res. 104(B11), 25611–25622.

THOMAS, J. C., CLAUDEL, M. E., COLLOMBET, M., TRICART, P., CHAUVIN, A. & DUMONT, T. 1999: First paleomagnetic data from the sedimentary cover of the French Penninic Alps: evidence for Tertiary counterclockwise rotations in the Western Alps. Earth and Planetary Science Letters 171, 561–574.

TRICART, P., SCHWARTZ, S., SUE, C., POUPEAU, G. & LARDEAUX, J.-M. 2001: La dénudation tectonique de la zone ultradauphinoise et l'inversion du front briançonnais au sud-est du Pelvoux (Alpes Occidentales): une dynamique miocène à actuelle. Bull. Soc. géol. France 172(1), 49–58.

VIALON, P., ROCHETTE, P. & MÉNARD, G. 1989: Indentation and rotation in the Alpine arc. In: COWARD, M.P., DIETRICH, D., PARK, R.G. Ed. Spec.-Alpine Tectonics. Geological Society of London 45(Special Publication), 329–338.

WAWRZYNIEC, T. F., SELVERSTONE, J. & AXEN, G. J. 2001: Style of footwall uplift along the Simplon and Brenner normal fault system, central and Eastern Alps. Tectonics 20(5), 748–770.

WUST, G. & SILVERBERG, D. 1989: Northern Combin zone complex-Dent Blanche nappe contact: extension within the convergent Alpine belt. Schweiz. mineral. petrogr. Mitt. 69, 251–259.

Manuscript received June 3, 2003
Revision accepted September 10, 2003